Alternative Characterization of Analog Signal Deformation for GNSS-GPS Satellites

Gabriel Wong, R. Eric Phelts, Todd Walter, Per Enge,
Stanford University

BIOGRAPHY

Gabriel Wong is an Electrical Engineering Ph.D. candidate at the Stanford University GNSS Research Laboratory. He has previously received an M.S.(EE) from Stanford University, and a B.S.(EECS) from UC Berkeley. His current research involves signal deformation monitoring and mitigation for GNSS signals.

R. Eric Phelts, Ph.D., is a research engineer in the Department of Aeronautics and Astronautics at Stanford University. He received his B.S. in Mechanical Engineering from Georgia Institute of Technology in 1995, and his M.S. and Ph.D. in Mechanical Engineering from Stanford University in 1997 and 2001, respectively. His research involves signal deformation monitoring techniques and analysis for SBAS, GBAS, and the GPS Evolutionary Architecture Study (GEAS).

Todd Walter, Ph.D., is a senior research engineer in the Department of Aeronautics and Astronautics at Stanford University. Dr. Walter received his Ph.D. from Stanford and is currently working on modernization of the Wide Area Augmentation System (WAAS) and defining future architectures to provide aircraft guidance. Key contributions include early prototype development proving the feasibility of WAAS, significant contribution to the WAAS MOPS, design of ionospheric algorithms for WAAS, and development of dual frequency algorithms for SBAS. He is a fellow of the Institute of Navigation and serves as its president.

Per Enge, Ph.D., is a professor of aeronautics and astronautics at Stanford University, where he is the Kleiner-Perkins Professor in the School of Engineering. He directs the GNSS Research Laboratory, which develops satellite navigation systems. He has been involved in the development of the Federal Aviation Administration's GPS Wide Area Augmentation System (WAAS) and Local Area Augmentation System (LAAS). For this work, Enge has received the Kepler, Thurlow, and Burka awards from the Institute of Navigation (ION). He received his Ph.D. from the University of Illinois. He is a member of the National Academy of Engineering and a Fellow of the IEEE and the ION.

ABSTRACT

Currently, analog signal deformation is described using individual-chip step response curves for each GPS/WAAS-GEO satellite. Such a set of curves is helpful – it allows us to have an overall idea of the distortions for all satellites as well as identify possibly anomalous satellite signals. However, the step response curves do not convey the severity of the distortions to the user in a metric he/ she can intuitively grasp. In addition, there is no current specification for nominal analog deformation. The ICAO model describes only the faulted mode.

In this paper, we propose an alternative method of characterizing nominal analog distortion: using the change in behavior of early-minus-late (EML) tracking errors across different correlator spacings. Such a measurement metric is more user-intuitive, and is directly related to user-domain parameters of interest such as pseudorange and position errors. In turn, these errors are of great importance to the performance and integrity of satellite-based augmentation systems (SBAS) and ground-based augmentation systems (GBAS).

Two different methods to obtain such tracking error curves are described and compared – processing of satellite dish antenna raw data and hardware GPS receiver outputs. Error sources affect the accuracy of our tracking error plots; for the satellite dish method these error sources and mitigation procedures are illustrative and discussed. The results from the two methods are presented and compared. The predicted inter-satellite tracking error plots are also compared to those observed from actual hardware receivers. For additional verification, results from the tracking error plots for particular correlator spacings are also compared to errors from actual hardware receiver pseudoranges with the same correlator spacings. Future work for both these methods is also proposed.

INTRODUCTION

Signal deformations for GNSS-GPS satellites have previously been classified based on the ICAO second-order step fault model**[1]**. This model has 3 parameters:
1. Δ: the amount of lead or lag in the falling edges of the distorted C/A code with respect to the expected position of those edges.
2. f_d: the ringing frequency associated with the edges of the distorted C/A code.
3. σ: the damping coefficient associated with that ringing.
[Δ pertains to digital distortion and f_d and σ pertain to analog distortion.]

The digital distortion parameter, Δ, is easily measured and its effects are well-understood. Thus, it is a convenient parameter to use in characterizing digital distortions of the GNSS-GPS satellite constellation. There is even a nominal range of values specified for Δ: between -10ns and +10ns.

Currently, analog signal deformation is described using individual-chip step response curves for each GPS/WAAS-GEO satellite **(Figure 1).**

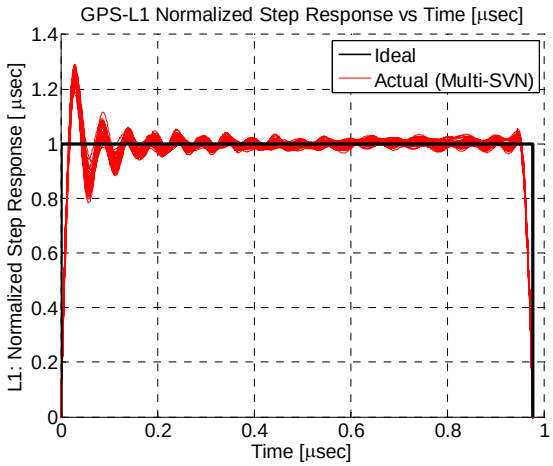

Figure 1: Analog distortion for all PRN satellites. Data collected in Aug 2008, Jul 2009, Aug 2010.

Such a set of curves is helpful – it allows us to have an overall idea of the distortions for all satellites as well as identify possibly anomalous satellite signals. However, the step response curves do not convey to the user how he/ she would be affected by the severity of the distortions. In addition, there is no current specification for nominal analog deformation; the ICAO model describes only the faulted mode.

In this paper, we propose an alternative method of characterizing analog distortion: using the change in behavior of early-minus-late (EML) tracking errors across different correlator spacings. Examples of such plots are presented in **Figure 2.**

The figure shows the differential pseudorange errors a mobile user would experience at various correlator spacings, for different GPS satellite signals, given a reference receiver correlator spacing of 1 chip.

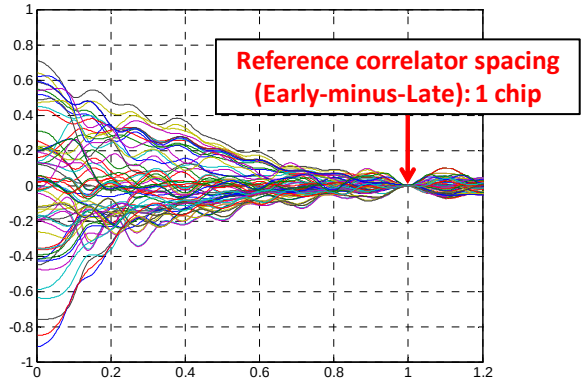

Figure 2: Example plot of tracking errors across different tracking loop Early-minus-Late (EML) correlator spacings, for different satellite signals.

Such a measurement metric is more intuitive, and is directly related to user-domain parameters of interest such as pseudo-range and position errors. In turn, these errors are of great importance to the performance and integrity of satellite-based augmentation systems (SBAS) and ground-based augmentation systems (GBAS).

In this paper, the new process(es) to obtain these curves will be described. These are based on data collected two different ways:
1. Data collection campaign of all GNSS-GPS and WAAS satellite signals using a 46m satellite dish antenna over a continuous 24-hour period.
2. All-in-view hardware GPS receivers with limited correlator outputs, over a 24-hour period.

We will begin by describing the processing for the satellite dish data as this is more involved.

The measured curves depend on the analog distortion caused by the measurement equipment. The effects of the ground equipment may change over time due to thermal changes or due to changes in equipment. The use of reference GNSS-GPS and WAAS satellite signals can remove these temporal changes and allow meaningful comparisons between satellite signals collected in different time periods. This process is described for the satellite dish data approach.

It is also important to note that common effects across all satellites affect only the timing accuracy and not the positioning accuracy. It is the satellite to satellite differences that are of greatest interest. Thus, we will also estimate and remove a common mode analog deformation

caused by the measuring equipment and similar behavior of the satellite filters.

These curves estimate what user receivers would experience in the absence of errors. The process for estimating some of these errors is presented, for the satellite dish data approach.

The hardware receiver approach contains some similarities and differences. The idea to obtain the tracking error plots is the same but the method is simpler as we do not have access to raw pre-correlation data. Instead, we only have correlator outputs at certain limited number of correlator spacings (typically less than 10). We use these outputs to obtain the tracking error plots and compare them with those from the satellite dish data.

The hardware receiver approach also allows us to configure a differential setup with specific correlator spacings and measure the double-difference pseudo-range errors. From these we derive the measured inter-satellite errors and compare them against the results from the tracking error plots. This serves as a simple verification of our tracking error plots.

Future work for both the satellite dish data approach and the hardware receiver approach will also be suggested.

SATELLITE DISH DATA PROCESSING METHOD

The tracking error plots are obtained by processing data from two different sources – satellite dish antenna and hardware. The method for processing satellite dish antenna data is as follows:

1. Data collection campaign.

This has been described previously**[4]**.

2. Data processing procedure
   This has also been described previously **[4]** and is briefly mentioned here:
   a. Use of high gain antenna
   b. Signal acquisition and tracking
   c. Multiple C/A code epoch averaging and interpolation for noise reduction
   d. Additional filtering for either noise reduction and/ or interpolation

The output of this process is an estimate of the actual received code chip waveform for all chips, for all GPS and WAAS-GEO satellite signals.

The difference here is that zero crossing locations for the formation of individual chips are not required; thus zero crossing determination methods are not applied unlike before.

3. Form points on correlation triangle by correlating received code chip waveform with ideal replicas at various delays and advances

Ideal replicas of various delays and advances of up to 1 chip are formed to correlate with the actual code chip waveform, for both GPS and WAAS-GEO satellite signals, to form correlator outputs. (In practice, given the large number of correlator output points available for our interpolated code chip waveform, the correlation is performed using the Fast Fourier Transform method).

In the example below in **Figure 3**, we use ideal replicas advanced and delayed by 0.1, 0.2, 0.3 and 0.4 chips to form early and late correlator outputs E1 and L1, E2 and L2, E3 and L3 and E4 and L4 at these chip spacings. Correlating the ideal replica without advances or delays with the received signal gives us the P (Prompt) correlator output.

P, E1-E4 and L1-L4 form discrete points on the correlation triangle (**Figure 4**). Using more finely spaced advanced and delayed ideal replica chip spacings produces the entire correlation triangle. The ideal correlation triangle, formed by correlating an ideal replica code (without advances or delays) with itself, is shown in blue. An example error-injected correlation "triangle", with artificially injected errors for illustration, is shown in red.

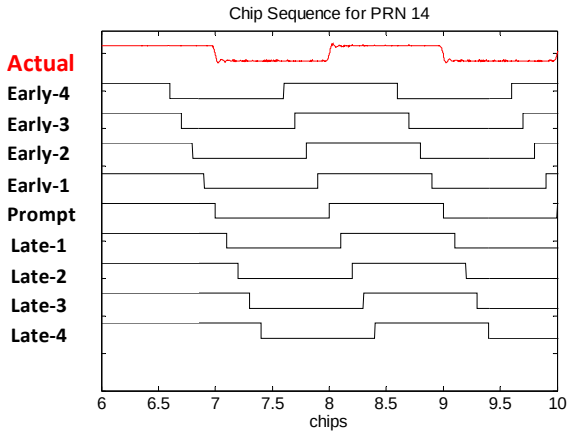

Figure 3: Form early, prompt and late replicas at different delays/ advances and correlate with actual code-sequence.

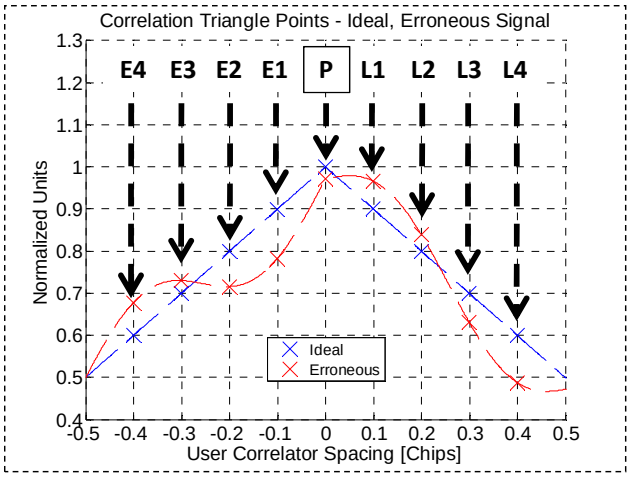

Figure 4: Points on correlation triangle for each different delay/ advance.

4. Subtract corresponding points, scale and plot with respect to horizontal separation (chips) between these points

With the points on the correlation triangle **(Figure 4),** we take differences of corresponding points (eg. E1 – L1, E2 – L2, E3 – L3 etc). Next we normalize and scale the differences. The scale factor K used to scale the normalized differences is computed as follows:

$$K = \frac{1}{2P} * \frac{1}{f_{CA}} * c \quad \text{---------- (1)}$$

where

f_{CA}: *frequency of GPS-L1C/A Code*

c: *speed of light*

P: *value of prompt (P) correlation*

Finally we plot the normalized and scaled differences against the absolute horizontal distance (chips) between the points. For instance, the absolute horizontal distance between E1 and L1 is abs(-0.1 – (+0.1)) chips = 0.2 chips. This produces the tracking error plots we are looking for. **Figure 5** shows the tracking error plot obtained using our ideal signal and signal with artificially injected errors.

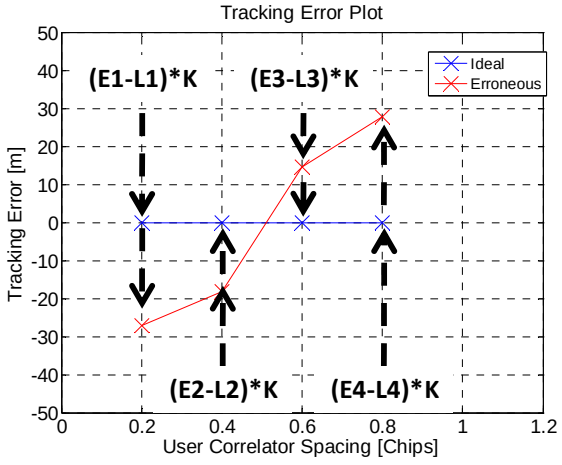

Figure 5: Tracking error plot for ideal and erroneous signals.

5. Choose a reference correlator spacing: vertically shift all tracking error curves (by adding different constants) so that they are zero at the reference correlator spacing.

This is chosen based on the desired/ applicable target environment. (For instance, 0.1 chips for WAAS). We do this because we are concerned about *differential errors* mobile users with different tracking loop correlator spacings experience for different satellites**.**

The following sets of tracking error curves are for reference correlator spacings of 0.1 chips and 1 chip, respectively **[Figure 6** and **7].**

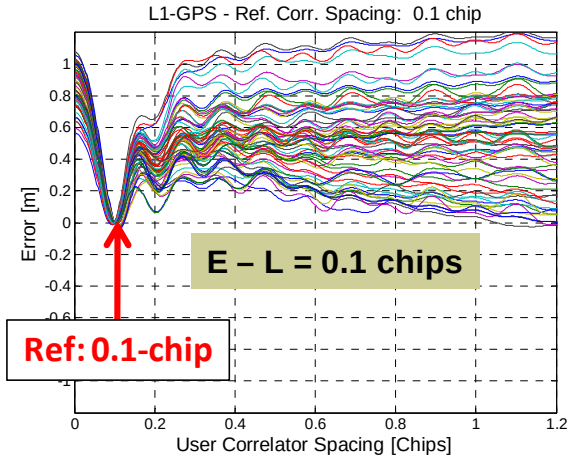

Figure 6: Tracking error curve for reference correlator spacing of 0.1 chips.

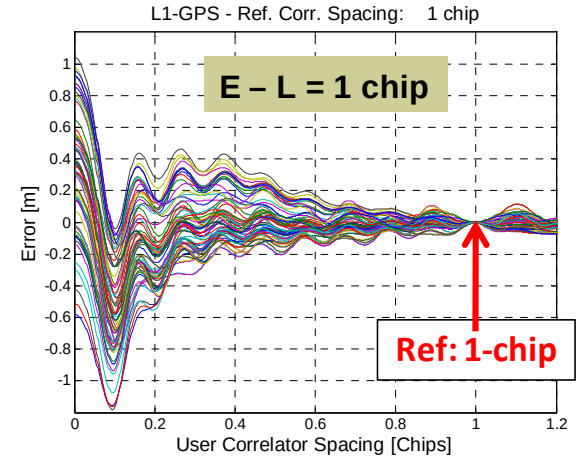

Figure 7: Tracking error curve for reference correlator spacing of 1 chip.

These two sets of curves are virtually identical. The difference is that each set is referenced to a different correlator spacing – all satellite curves are shifted vertically via additive constants so that all the resulting curves for a set are identically zero at the reference correlator spacing [0.1chip for **Figure 6** and 1 chip for

Figure 7]. The curves also show very similar variation from satellite to satellite across a set.

6. Removal of common mean (after correction for errors such as time-varying biases)

Since we are interested in inter-satellite biases and their effect on the navigation solution, we subtract the common mean from the tracking error plots. (This would only affect timing but not the navigation solution). This step is only performed after the correction for errors such as time-varying biases (described in the next section) has been performed.

These curves show the estimated errors differential mobile users would experience. How accurate these tracking error plot estimates are depends on the errors in the measurement process. We will discuss two sources of these errors – time-varying biases and instantaneous random errors in subsequent sections.

TIME-VARYING BIASES – MITIGATION USING COMMON WAAS-GEO SATELLITE SIGNALS

In this section we discuss the effect and mitigation procedures for time-varying biases which affect our tracking error plots.

The satellite dish data was collected in 4 time periods on Aug 3-4 2010

1. Aug 4 UTC 0-4 hours (PST 5pm-9pm Aug 3)
2. Aug 4 UTC 7-10 hours (PST 12am-3am Aug 4)
3. Aug 4 UTC 14-16 hours (PST 7am-9am Aug 4)
4. Aug 4 UTC 21-23 hours (PST 2pm-4pm Aug 4)

Different time-varying biases can be seen in the tracking error plots for the different time periods (**Figure 8**). Compared to time period 1 (**Figure 8a**), tracking error plots for time periods 2 and 3 (**Figures 8b** and **8c**) seem to have a negative bias at some correlator spacings, while time period 4 (**Figure 8d**) seems to have a positive bias.

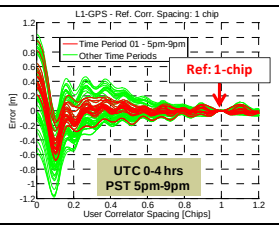

Figure 8a: Time period 1 highlighted.

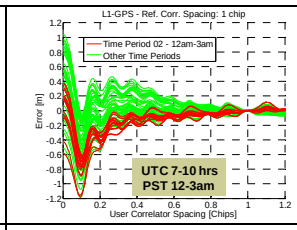

Figure 8b: Time period 2 highlighted.

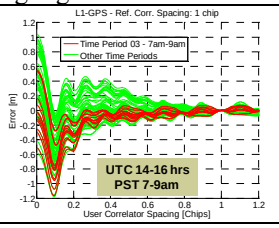

Figure 8c: Time period 3 highlighted.

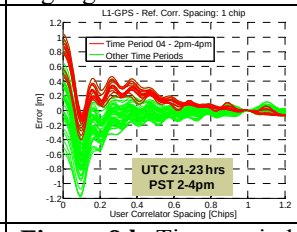

Figure 8d: Time period 4 highlighted.

Figure 8: Tracking error plots for data collected at different times of day. Tracking error plots for the entire day are in green, while tracking error plots for the time period of interest are highlighted in red. Time-varying biases are visible.

If we could remove these time-varying biases, we would be able to obtain a more accurate set of tracking error plots. Average differences between WAAS-GEO satellite signals, also collected in the same periods, were used as an estimate of the inter-time-period biases (**Figure 9**).

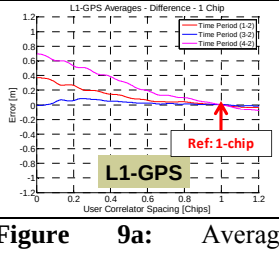

Figure 9a: Average difference between GPS signals in time periods 1, 3, 4 and time period 2.

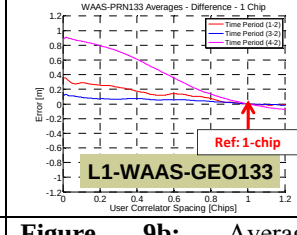

Figure 9b: Average difference between WAAS-GEO PRN133 signals in time periods 1, 3, 4 and time period 2.

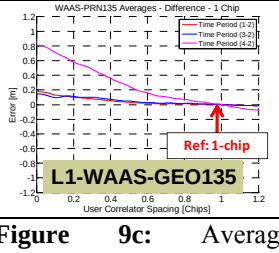

Figure 9c: Average difference between WAAS-GEO PRN135 signals in time periods 1, 3, 4 and time period 2.

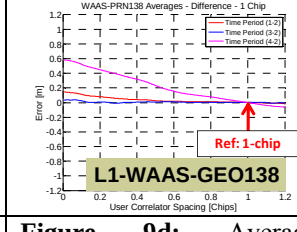

Figure 9d: Average difference between WAAS-GEO PRN138 signals in time periods 1, 3, 4 and time period 2.

Figure 9: Average differences between tracking error plots for time periods 1, 3 and 4 and that for time period 2, for GPS and individual WAAS-GEO satellite signals.

These estimates of time-varying biases were used as corrections for the inter-time-period biases for the GPS signals. These difference curves are not identical in the 4 cases, but have differences of up to ±0.2m. This could possibly be due to thermal effects on the satellite dish, signal feedhorn and filter, in addition to the signal data not being collected simultaneously.

Applying these corrections yields the following tracking error plots (**Figure 10**). The time-varying biases observed previously are now substantially removed.

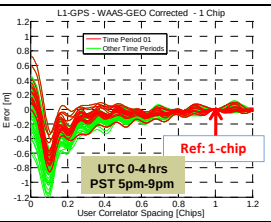

Figure 10a: Time period 1 highlighted.

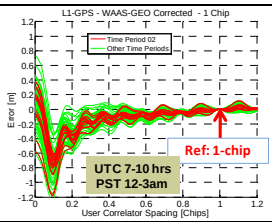

Figure 10b: Time period 2 highlighted.

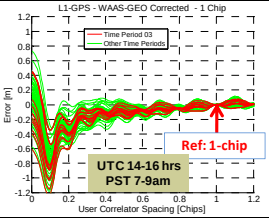

Figure 10c: Time period 3 highlighted.

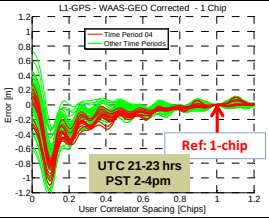

Figure 10d: Time period 4 highlighted.

Figure 10: Tracking error plots for data collected at different times of day. Tracking error plots for the entire day are in green, while tracking error plots for the time period of interest are highlighted in red. The time-varying biases look substantially removed after application of the corrections from WAAS-GEO satellites.

Since we are interested in inter-satellite biases and their effect on the navigation solution, we subtract the common mean from all corrected tracking error plots. (This would only affect timing but not the navigation solution). The results are shown in **Figure 11**.

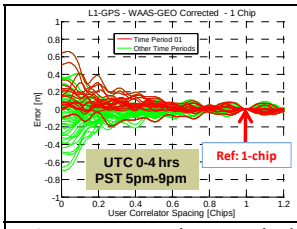

Figure 11a: Time period 1 highlighted.

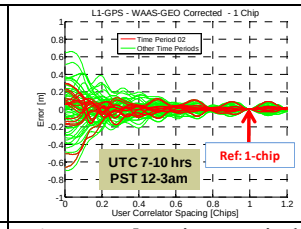

Figure 11b: Time period 2 highlighted.

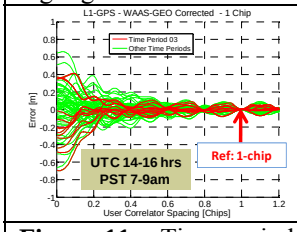

Figure 11c: Time period 3 highlighted.

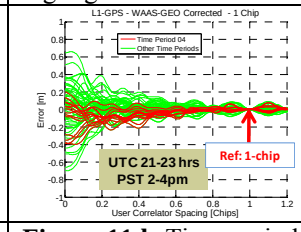

Figure 11d: Time period 4 highlighted.

Figure 11: Tracking error plots after application of corrections for time-varying biases and removal of common mean. Tracking error plots for the entire day are in green, while tracking error plots for the time period of interest are highlighted in red.

The following table shows the worst case and root-mean-square (RMS) error for the entire set of GPS signals, before and after applying the corrections for time-varying bias. Both the worst case and RMS errors are reduced from before.

$$\text{RMS error} = \sqrt{\frac{\sum_{i}\sum_{\tau_c}[z_i(\tau_c)]^2}{N_{SV} * N_{\tau c}}} \text{ [m]} \qquad \text{----------(1)}$$

Where

τ_c : *User Correlator Spacing[chips]*
i : *Index of Satellite*
$z_i(\tau_c)$: *Tracking error curve for satellite i*
N_{SV} : *Number of satellite tracking error curves*
$N_{\tau c}$: *Number of different user correlator spacings*

Worst error error

$$= \max_{\tau_c}(\max_{i}\{z(\tau_c, i)\} - \min_{j}\{z(\tau_c, j)\}) \text{[m]} \text{ ---(2)}$$

Where

τ_c : *User Correlator Spacing[chips]*
i, j : *Index of Satellite*
$\{z_i(\tau_c)\}, \{z_j(\tau_c)\}$: *Set of tracking error curves*

	RMS [m] Error	Worst Case Error [m]
Before WAAS correction	0.126	1.62
After WAAS correction	0.083	1.36

Table 1: Worst case error [m] and root-mean-square (RMS) [m] for the GPS signals.

What are the inherent errors in our satellite dish data measurement process? This would affect the accuracy of the tracking error plots, both in the tracking error plots of the GPS signals, which we are more interested in, as well as the WAAS-GEO satellite signals, which were used to derive corrections for the time-varying biases. The magnitude of these errors and how they are estimated are discussed in the next section.

MEASUREMENT PROCESS ERRORS (AFTER REMOVAL OF TIME-VARYING BIASES)

To have an estimate of the instantaneous random errors in the measurement process, for each satellite signal we collected a pair of measurements a short time (2-3 minutes) apart and processed them to obtain tracking error curves. The worst-case error and root-mean-square (RMS) between these tracking error curves give an estimate of the error in our measurement process. These are shown in **Figure 12**.

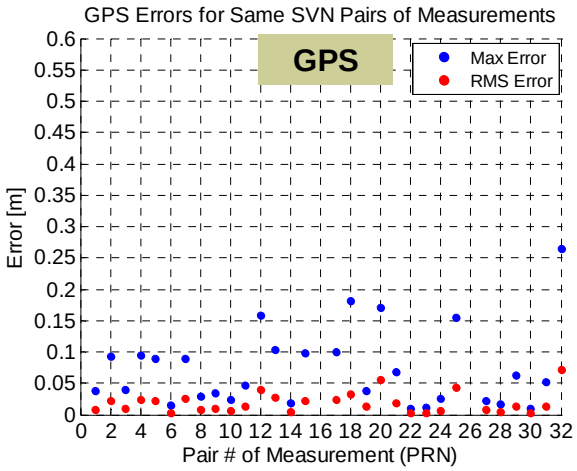

Figure 12: Worst-case and RMS errors between each pair of **GPS** same-satellite tracking error curves. Data was taken a short time (2-3 minutes) apart.

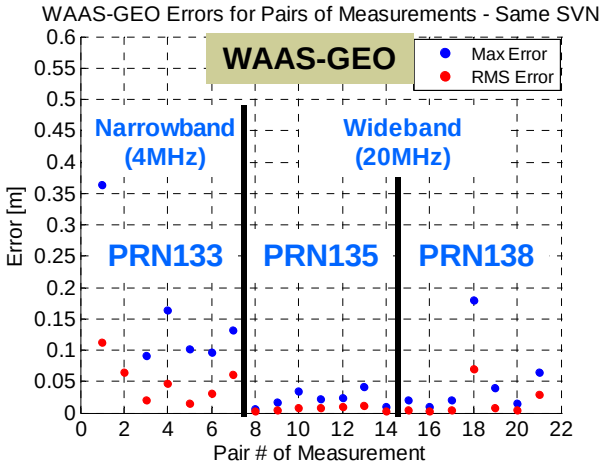

Figure 13: Worst-case and RMS errors between each pair of **WAAS-GEO** same-satellite tracking error curves. Each pair of curves was based on data taken a short time (2-3 minutes) apart.

$$\text{RMS error(i)} = \sqrt{\frac{\sum_{\tau_c}\left(z_i^1(\tau_c) - z_i^2(\tau_c)\right)^2}{N_{\tau c}}} \text{ [m] ---------(3)}$$

Where

τ_c : *User Correlator Spacing[chips]*
i : *Index of Satellite*
$z_i^1(\tau_c)$: *First tracking error curve for satellite i,*
$z_i^2(\tau_c)$: *Second tracking error curve for satellite i*
$N_{\tau c}$: *Number of different user correlator spacings*

$$\text{Worst case error(i)} = \max_{\tau_c}\left(abs\left(z_i^1(\tau_c) - z_i^2(\tau_c)\right)\right) \text{ [m]}$$

----------(4)

Where

τc : *User Correlator Spacing[chips]*
i : *Index of Satellite*
$z_i^1(\tau_c)$: *First tracking error curve for satellite i,*
$z_i^2(\tau_c)$: *Second tracking error curve for satellite i*

	RMS Error [m]	Worst Case Error [m]
GPS	0.07	0.26
WAAS-GEO #133 (narrowband)	0.15	0.36
WAAS-GEO #135, #138 (wideband)	0.06	0.12

Table 2: Worst case error [m] and root-mean-square (RMS) errors [m] for the set of GPS and WAAS-GEO signals

RMS measurement errors for the GPS and wideband WAAS-GEO tracking error plots are generally small but the worst case errors are larger. As would be expected, the

narrowband WAAS-GEO PRN133 signal has larger deviations. These errors give an estimate of the accuracy of our GPS tracking error plots with WAAS-GEO corrections applied.

COMPARISON WITH HARDWARE RECEIVER

The tracking error plots in the previous sections showed the errors differential user receivers experience relative to a reference receiver, given different correlator spacings and for different satellites. In this section, we examine how well the estimates obtained using satellite dish data compare to that from actual hardware receivers.

We use two methods of comparison: tracking error plots based on discriminator pairs and resultant double-difference pseudo-range biases for pairs of receivers with different tracking loop correlator spacings.

The first method requires receivers with special correlator outputs, while the second method requires receivers which have variable settings for correlator spacing. For our comparison, we used three Novatel Propak receivers with Signal Quality Monitoring correlator outputs. Data was collected Dec 3-5 2010.

1. Tracking error plots based on discriminator pairs

This method is similar to what was described before – scaled differences between Early-minus-Late correlator pairs. The main differences are that in the case of the hardware receiver, the number of discriminator pairs is usually very limited (less than 10). This results in limited points of the tracking error curve. Typically there is also higher noise at the receiver due to use of an all-in-view omni-directional antenna, and also some possible multipath.

We use the approach as outlined in SATELLITE DISH DATA PROCESSING METHOD. Only step 4: "**Subtract corresponding points, scale and plot with respect to horizontal separation (chips) between these points**" is required. (The hardware receiver performs steps 1-3 and 5 – choice of referece correlator spacing – is pre-set ahead of time.)

In addition, tracking error plots from the receiver are averaged over an hour for noise reduction.

Figures 14 and **15** show the tracking error plots for the same correlator spacing. The common mean has been removed.

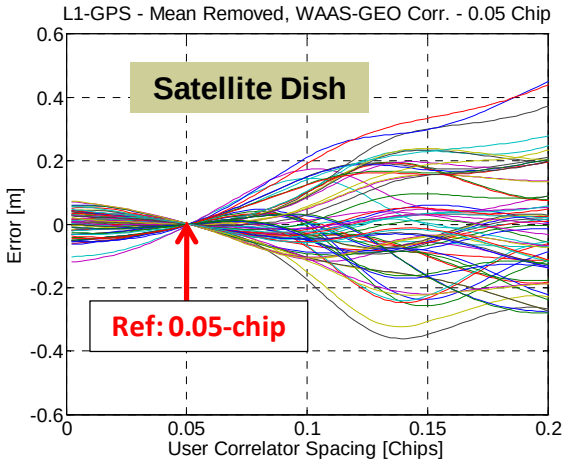

Figure 14: GPS Tracking error plots obtained using satellite dish data.

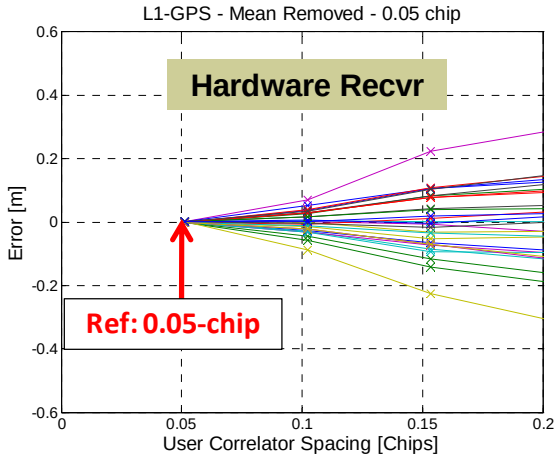

Figure 15: GPS Tracking error plots obtained from hardware receiver limited correlator points.

These graphs show that the two set of curves have similar trends but actual values do not correspond exactly. These and other discrepancies will be discussed in a subsequent section.

2. Biases using double-difference pseudo-ranges for pairs of receivers with different correlator spacings

For this comparison, three hardware receivers received signals via a splitter connected to the same antenna. Two of them were set to the **ULTRANARROW correlator setting (correlator spacing of 0.05115 chips)** as a control while the third was set to the **NARROW correlator setting (correlator spacing of 0.1023 chips).**

Two sets of double-difference pseudoranges were formed – one set between receivers of the same correlator spacing settings as a control, and another set between receivers of different correlator spacing settings.

The set of detailed equations for both these sets of double differences, including noise terms, can be found in Appedix A.

Briefly, there are three residual noise terms which affect the double-difference biases between receivers in a differential configuration: multipath, analog distortion and receiver thermal noise. Digital distortions of up to 4ns have an effect of at most 0.01m in the differential receiver configuration. Virtually all GPS satellites have digital distortions comfortably in this range; thus digital distortion effects can be safely omitted from consideration.

For two receivers which have the same tracking loop correlator spacing, the multipath and analog distortion effects on the double-difference pseudo-ranges would be identical and cancel. What would be left would be twice that of the receiver thermal noise. For two receivers which have different tracking loop correlator spacings, multipath and analog distortion would have dissimilar effects and result in non-zero biases. Using carrier-smoothing with long time constant smoothing filter (900 seconds) would eliminate the multipath and receiver thermal noise.

Based on which common satellites are used in the double-differences, we can form leveling matrices[**5**]. Together with the inter-satellite biases we obtained, we can solve the systems of equations in a least-squares fashion to get tracking errors for all the satellites (**Figures 17 and 18)**. Ideally these would match our estimates using the tracking error plots from our satellite dish data processing (**Figure 16)**, for the same set of correlator spacings. For the receiver configuration with different correlator spacings, both the satellite dish data estimated errors and the actual hardware observed errors are overlaid on the same plot for easier comparison **(Figure 19**).

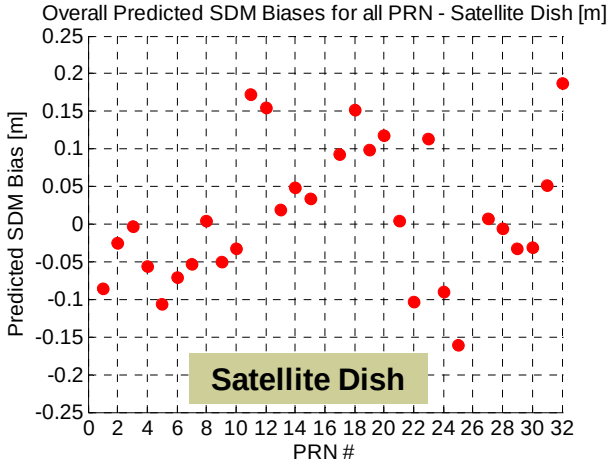

Figure 16: Estimated tracking errors from satellite dish data. Reference receiver at correlator spacing of 0.05chips; mobile user receiver at correlator spacing of 0.1chips.

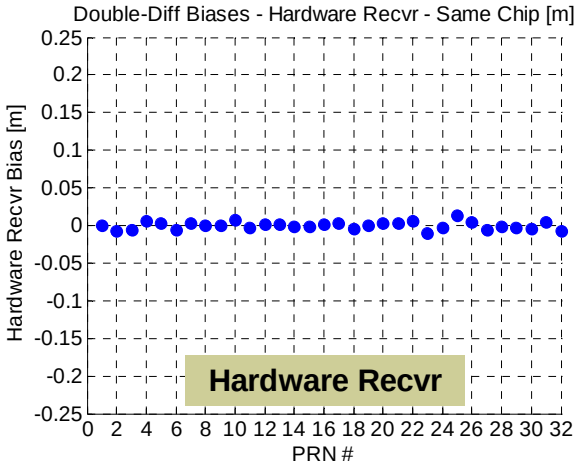

Figure 17: Estimated tracking errors from hardware receiver. Both reference and mobile user receivers have tracking loop correlator spacings of 0.05chips.

Figure 17 shows that the average biases are very close to zero for different receivers both set to the same tracking loop correlator spacing.

Figures 18 and **19** show that there is some correspondence between estimated tracking errors for the satellite dish and from the double-difference pseudoranges – some of the errors are virtually identical and they have the same order of magnitude. Most of the values do not correspond, possibly due to uncharacterized errors.

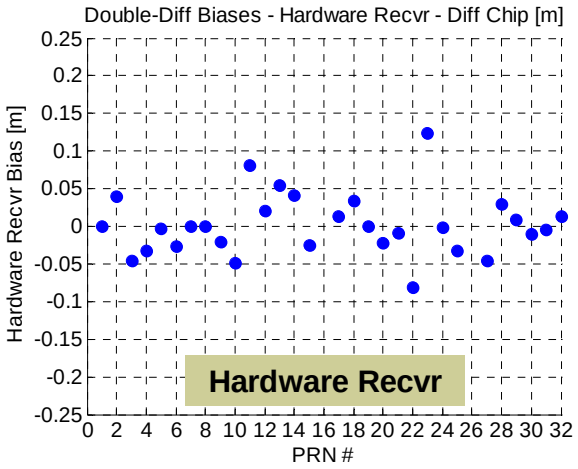

Figure 18: Estimated tracking errors from hardware receiver. Reference receiver tracking loop correlator spacing is 0.05chips; mobile user receiver tracking loop correlator spacing is 0.1 chips.

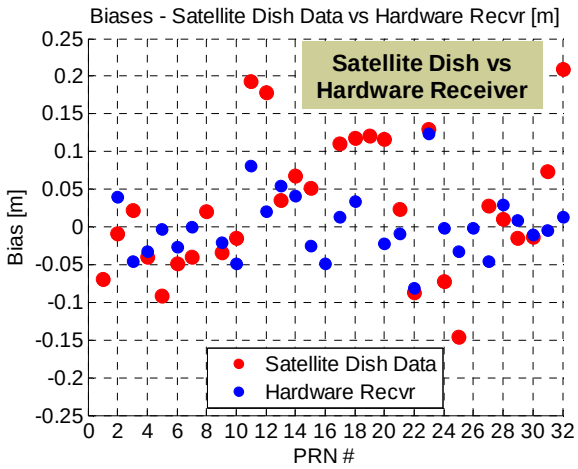

Figure 19: Comparison of estimated tracking errors obtained from satellite dish data and hardware receiver. Reference receiver at correlator spacing of 0.05chips; mobile user receiver at correlator spacing of 0.1chips.

SUMMARY OF DIFFERENCES IN APPROACHES

There were some discrepancies between the tracking error plots for the satellite dish data and the hardware receiver approaches. In addition there were also some discrepancies between what was estimated using the tracking error plots and what was obtained using double-difference pseudorange biases.

The discrepancies are likely caused by the differences in the satellite dish and the hardware receiver data collection approaches. In this section we summarize these differences, and highlight how they could result in the discrepancies.

Satellite Dish	Hardware Receiver
• 1 satellite at a time, 2secs. • Very high gain, low noise.	• All in view, continuous. • Average over hours for noise reduction.
Advantages: • Overall picture – analog step response, tracking error plots	Advantages: • Cheap, easy access, not time-consuming
Disadvantages: • Expensive • Time consuming • As-yet un-characterized error in data collection	Disadvantages: • More noisy • Output depends on receiver filter and multipath at site • Limited correlator points • Use of special-output receiver required

Table 3: Summary of differences between the satellite dish and hardware receiver approaches

Looking at **Table 3**, we see that the satellite dish and hardware receivers are two very different approaches. For the satellite dish approach, we collect high-gain, high-bandwidth low-noise 2sec snapshots, one satellite at a time to create the tracking error plots. These tracking error plots are thus based on short-duration data taken at different times. On the contrary, the hardware receiver collects lower-gain data in a continuous fashion, simultaneously for multiple satellites, and results are then averaged over a longer duration (1 hour) for noise reduction.

Our examination of the noise in our measurement process also suggests that our results could be obscured to a certain extent by noise. Some possible sources of this noise are uncharacterized noise at the dish and filter effects at the receiver.

FUTURE WORK

Our future work with regard to the satellite dish data approach would involve data collection from satellite dishes with better characterization of signal properties such as filter and noise characteristics. For the hardware receiver approach, we hope to collect data from different receivers at different sites for comparison.

CONCLUSION

In this paper, we presented our work in forming an alternative characterization of analog signal deformation for GNSS-GPS satellites – using tracking error plots. These plots present analog signal distortions and their impact on the user in a way that is more intuitive. Two approaches were used and presented – the satellite dish data and hardware receiver data approaches – as well as the processes involved for these approaches.

For more accurate characterization, time-varying biases were identified and mitigated against, for the illustrative case of the satellite dish data. Worst case and root-mean-square (RMS) errors in the measurement process were examined, which give an estimate of how accurate our tracking error plots are.

Actual hardware receivers were also used for verification of both the tracking error plots as well as the biases as estimated by the tracking error plots.

Our work as presented shows that the use of tracking error plots is an intuitive and effective way to provide a basis for characterization and specification of the quality of GPS-GNSS satellite signals, from the perspective of analog signal distortion. The two approaches to derive these curves are straightforward. It is also possible to verify these tracking error plots with actual hardware.

These plots as obtained using current approaches do contain error; future work would attempt to understand better and characterize this error.

REFERENCES

[1] Mitelman, A., "Signal quality monitoring for GPS augmentation systems", Ph.D. Dissertation, Stanford University, December 2004

[2] Phelts, R.E., "Multicorrelator Techniques for Robust Mitigation of Threats to GPS Signal Quality", Ph.D. Dissertation, Stanford University, June 2001

[3] Phelts, R. E., Walter, T., Enge, P., "Characterizing Nominal Analog Signal Deformations on GNSS Signals", ION-GNSS2009

[4] Wong., G., Phelts, R. E., Walter, T., Enge, P., "Characterization of Signal Deformations for GPS and WAAS Satellites", ION-GNSS2010

[5] Strang, G., Borre, K., "Linear Algebra, Geodesy, and GPS", Chapter 8: Levelling Networks, Wellesley College (1997)

[6] Misra, P., Enge, P., "Global Positioning System – Signals, Measurements and Performance", Ganga-Jamuna Press (2nd 2006)

APPENDIX: DOUBLE DIFFERENCE EQUATIONS

Equations for pseudoranges [**6**]:

$$\rho = r + c[\delta t_u - \delta t^s] + I_\rho + T_\rho + \varepsilon_\rho + MP_\rho + SDM_\rho \quad \text{----------(5)}$$

Where

ρ: *Pseudorange*
c: *Speed of light*
δt_u: *User clock bias in seconds*
δt^s: *Satellite clock bias in seconds*
I_ρ: *Ionospheric error in pseudorange domain in meters*
T_ρ: *Tropospheric error in pseudorange domain in meters*
ε_ρ: *Receiver thermal noise error in pseudorange domain in meters*
MP_ρ: *Multipath error in pseudorange domain in meters*
SDM_ρ: *Signal distortion error in pseudorange domain in meters*

Receivers with different chip spacing (general case):
Single pseudorange difference

$$\rho_{mn} = c[\delta t_{u,m} - \delta t_{u,n}] + \varepsilon_{\rho,m} - \varepsilon_{\rho,n} + MP_{\rho,m} - MP_{\rho,n} + SDM_{\rho,m} - SDM_{\rho,n} \quad \text{----------(6)}$$

Where
m,n: subscripts of hardware receivers

Double pseudorange difference

$$\rho_{mn}^{ij} = \varepsilon_{\rho,mn}^{ij} + MP_{\rho,mn}^{ij} + SDM_{\rho,mn}^{ij} \quad \text{----------(7)}$$

$$\rho_{mn}^{ij} = (\rho_m^i - \rho_n^i) - (\rho_m^j - \rho_n^j) \quad \text{----------(8)}$$

$$\varepsilon_{\rho,mn}^{ij} = (\varepsilon_{\rho,m}^i - \varepsilon_{\rho,n}^i) - (\varepsilon_{\rho,m}^j - \varepsilon_{\rho,n}^j) \quad \text{----------(9)}$$

$$MP_{\rho,mn}^{ij} = (MP_{\rho,m}^i - MP_{\rho,n}^i) - (MP_{\rho,m}^j - MP_{\rho,n}^j) \quad \text{----------(10)}$$

$$SDM_{\rho,mn}^{ij} = (SDM_{\rho,m}^i - SDM_{\rho,n}^i) - (SDM_{\rho,m}^j - SDM_{\rho,n}^j) \quad \text{----------(11)}$$

Where
m,n: subscripts of hardware receivers
i,j: subscripts of satellites

If $\varepsilon_{\rho,mn}^{ij}$ and $MP_{\rho,mn}^{ij}$ are small relative to SDM biases, we can see $SDM_{\rho,mn}^{ij}$, which are the relative SDM biases between different satellites.

Since SDM biases are constant over time, we can also average $\varepsilon_{\rho,mn}^{ij}$ and $MP_{\rho,mn}^{ij}$ a over a long duration of time, say an hour, to reduce $\varepsilon_{\rho,mn}^{ij}$ and $MP_{\rho,mn}^{ij}$ further.

[Assumption: $\varepsilon_{\rho,mn}^{ij}$ and $MP_{\rho,mn}^{ij}$ are zero mean random variables].

For receivers with same chip spacing:
Single pseudorange difference

$$\rho_{mn} = c[\delta t_{u,m} - \delta t_{u,n}] + \varepsilon_{\rho,m} - \varepsilon_{\rho,n} \quad \text{----------(12)}$$

Note that the MP and SDM error terms are cancelled.

Double pseudorange difference

$$\rho_{mn}^{ij} = \varepsilon_{mn}^{ij}$$

In this case, as a control, we should see that ρ_{mn}^{ij} should be zero-mean over a long duration of time, say an hour.